# *Experiments on the Biporous Micropillar Array for Enhanced Heat Transfer Performance*



**Citation:** He, Bin, Mengyao Wei, Qian Liang, Chuan Seng Tan, and Evelyn N. Wang. "Experiments on the Biporous Micropillar Array for Enhanced Heat Transfer Performance." Volume 2: Micro/Nano-Thermal Manufacturing and Materials Processing; Boiling, Quenching and Condensation Heat Transfer on Engineered Surfaces; Computational Methods in Micro/Nanoscale Transport; Heat and Mass Transfer in Small Scale; Micro/Miniature Multi-Phase Devices; Biomedical Applications of Micro/Nanoscale Transport; Measurement Techniques and Thermophysical Properties in Micro/Nanoscale; Posters (January 4, 2016).

**As Published:** http://dx.doi.org/10.1115/MNHMT2016-6430

**Publisher:** ASME International

**Persistent URL:** http://hdl.handle.net/1721.1/120325

**Version:** Final published version: final published article, as it appeared in a journal, conference proceedings, or other formally published context

**Proceedings of the ASME 2016 5th International Conference on Micro/Nanoscale Heat and Mass Transfer**
**MNHMT2016**
**January 4-6, 2016, Biopolis, Singapore**

# MNHMT2016-6430

# EXPERIMENTS ON THE BIPOROUS MICROPILLAR ARRAY FOR ENHANCED HEAT TRANSFER PERFORMANCE

**Bin He**
[1]Singapore-MIT Alliance for Research and Technology (SMART) Centre, Singapore

**Mengyao Wei**
[1]Singapore-MIT Alliance for Research and Technology (SMART) Centre, Singapore
[2]School of Electrical and Electronics Engineering, Nanyang Technological University, Singapore

**Qian Liang**
[1]Singapore-MIT Alliance for Research and Technology (SMART) Centre, Singapore

**Chuan Seng Tan**
[1]Singapore-MIT Alliance for Research and Technology (SMART) Centre, Singapore
[2]School of Electrical and Electronics Engineering, Nanyang Technological University, Singapore
Email: TanCS@ntu.edu.sg

**Evelyn N.Wang**
[1]Singapore-MIT Alliance for Research and Technology (SMART) Centre, Singapore
[3]Department of Mechanical Engineering, Massachusetts Institute of Technology, Cambridge, United States,
Email: enwang@mit.edu

## ABSTRACT

*A mathematical model has been developed in previous work to optimize the parameters of the biporous structures with micro channels among pillars to reduce the viscous force by shortening the liquid prorogation length inside porous media. In this paper, an experimental rig has been built to test the performance of the designed samples at ambient conditions according to the previous derived mathematical model. The pillar areas of the samples have been fabricated by photolithograph and Deep Reactive-Ion Etching (DRIE) with varied parameters for further comparisons. To simulate the concentrated heating of a working device and measure its temperature, a Pt heater and four Resistance Thermal Detectors (RTDs) have been fabricated by the electron beam deposition and lift-off process. The sample has been mounted horizontally to a water-proof sample holder, and the de-ionized water has been pumped into the evaporator through a reservoir by a syringe pump. By fine tuning the pumping rate, one can reach the minimum pumping rate while maintaining the water levels of the reservoir and the evaporator without drying out for a certain heating power. The mathematical model has be partially verified by the experimental results, which paves the way for the final design of the silicon vapor chamber.*

## NOMENCLATURE

$L$ Half of total wick length, $m$
$K$ Permeability of planar post array, $m^2$
$d$ Pillar diameter, $\mu m$
$h$ Pillar height, $\mu m$
$l$ Pitch (center to center distance), $\mu m$
$q''$ Maximum heat flux , $W/cm^2$
$rf$ Roughness factor of DRIE Si surface , $\pi/2$

$\theta$ Contact angle of water on Si surface, $^\circ$
$\varepsilon$ Porosity
$\delta$ Surface tension of water, $N/m$
$\rho$ Density , $kg/m^3$
$\mu$ Dynamic viscosity, $Pa \cdot s$
$A_m$ Actual meniscus area, $m^2$
$A_p$ Projected meniscus area, $m^2$
$P_{cap}$ Capillary pressure, $Pa$
$h_{fg}$ Latent heat of vaporization of water, $j/kg$
$k_{eff}$ Effective thermal conductivity, $W/m \cdot K$
$l_i$ Half island width, $\mu m$
$w_i$ Half microchannel width, $\mu m$
$\Delta E$ Decrease in surface energy as liquid fills one unit cell
$\Delta T$ Superheat, $^\circ C$
$\Delta V$ Volume of liquid filling one cell

## 1 Introduction

The rapid development of the integrated microelectronic device demands a compatible yet powerful cooling method. As a novel cooling technology, the silicon vapor chamber adopts the phase change mechanism and capillary flow to dissipate large amounts of concentrated heat at the evaporation area [1–3]. The capillary pressure is related to the shape of the interfacial area between the liquid and vapor phases, which can be altered by varying microstructure [4–7]. In the traditional configuration, sintered metal powders [8–12], nanotubes [13] and micro pillar array have been widely used to increase the liquid prorogation. By virtue of the advanced Microelectromechanical systems (MEMS) technology, diverse shapes and arrangements of micro pillars can be created conveniently in order to increase the capillary flow and thin film evaporation region at the evaporator to maximize its heat flux [2, 3, 14, 15].

The biporous structures with two different pore sizes has been added to the design of evaporator, and according to Wang et al. [16], the larger pore in the biporous structures can function as vapor duct to enhance evaporation. Semenic et al. have studied the Cu sintered power biporous wick with large (400 $\sim$710 $\mu m$) and small (53 $\sim$63 $\mu m$) pore diameters to achieve a critical heat flux of 990 $W/cm^2$, comparing with 300 $W/cm^2$ for a monoporous wicks [17–19]. In addition, for a uniformed microstructure, the maximum heat flux decreases with the propagation length of the liquid at the evaporator. The biporous structures with micro channels among pillars can reduce the viscous force by shortening the liquid flow inside porous media [20]. However, most of the evaporation happens at the thin film area of the micro pillars, the introduction of micro channels could potentially reduce the total heat flux of the evaporator. Therefore, a mathematical model has been developed to optimize the parameters of the biporous structures [20].

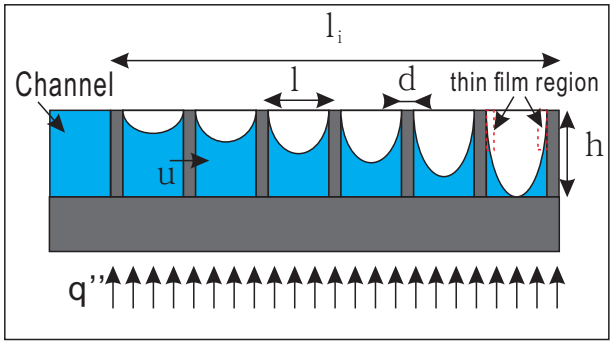


**FIGURE 1**. SCHEMATIC ILLUSTRATION OF A CAPILLARY WICK CONSISTS OF MICROPILLAR ARRAY.

### 1.1 Brief introduction of the analytical model

To simplify the problem, only results of the one dimensional (1D) samples will be investigated in the current study. The details of this analytical model have been discussed by Wei et al. [20]. The water propagation inside a porous media is induced by capillary pressure, and for micro-pillar structure, the capillary pressure can be calculated from the thermodynamic definition of pressure. According to Xiao et al. [21], pressure is equal to energy per unit volume, and the surface energy can be calculated from the simulation of the shape of the meniscus from the Surface Evolver [22].

$$P_{cap} = \frac{\Delta E}{\Delta V} = \frac{\sigma r f \cos\theta \pi dh + \sigma \cos\theta A_p - \sigma A_m}{\Delta V} \tag{1}$$

As shown in the Fig. 1, the 1D model for water propagating on the uniform pillar area with heating from below has been solved by Liang et al. [23] by considering water flows from the reservoir to the center of the pillar area driven by capillary force caused by different meniscus shapes among the pillar area due to evaporation. By solving the Brinkman equation, the max heat flux, $q''$ of the uniform pillar area can be expressed as

$$q'' = \frac{2P_{cap}\rho_l h_{fg} hK}{\mu {l_i}^2}\left[1 - \frac{\tanh(\sqrt{\frac{\varepsilon}{K}}h)}{\sqrt{\frac{\varepsilon}{K}}h}\right] \tag{2}$$

where $l_i$ is the propagation length, $K$ is the permeability, $h$ is the the pillar height. The propagation length is the most convenient parameter to alter during the design of the pillar structure, and shortening the propagation length can increase the heat flux dramatically. Consequently, a biporous structure has been proposed to add liquid channels for liquid to flow inside as a reservoir to minimize the propagation distance, as shown in the Fig. 2. The flow inside the micro channel has been solved numerically by

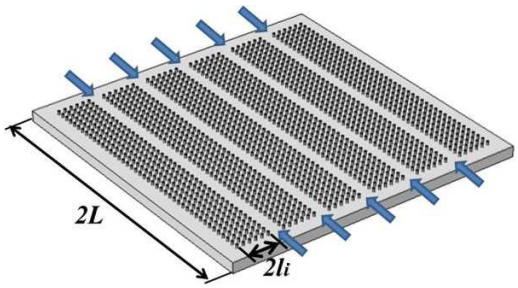


**FIGURE 2**. A 1D SIMPLIFICATION OF ISLANDS MICROPILLAR CONFIGURATION

assuming a pressure driven laminar flow inside a channel with porous side walls. The heat transfer model has been solved in in Wei et al. [20] by coupling the flow inside the channels with the evaporation inside the pillar area, and the heat flux can be written as

$$q'' = \frac{\frac{2\rho_l h_{fg} hK}{l_i \mu}\left[1 - \frac{\tanh(\sqrt{\frac{\varepsilon}{K}}h)}{\sqrt{\frac{\varepsilon}{K}}h}\right]\frac{1}{l_i+w}P_{cap}}{1 + \frac{2hK}{l_i^2}\left[1 - \frac{\tanh(\sqrt{\frac{\varepsilon}{K}}h)}{\sqrt{\frac{\varepsilon}{K}}h}\right]\frac{1}{l_i+w}\frac{L^2}{whf(\frac{w}{l_i},\frac{h}{l_i})}} \quad (3)$$

Based on the energy balance, the diameter, $d$, pitch, $l$, height of the micro pillars, $h$, and both widths of the pillar and channel areas, $l_i$ and $w_i$ can be optimized from Eqn. (3) according to the design and constrains. In this work, the micropillar samples designed by the analytical model has been fabricated and tested in order to provide some validations to the model.

## 2 Experiments

### 2.1 Sample fabrication

The process of fabrication can be seen in the Fig. 3. The 6" silicon wafer has been cleaned by SC-1 process for 20 minutes and dipped into HF solution (2.45 %) for 1 minute to remove any contaminants, and it has been sent to the oxidation furnace for thermal oxide growth at 900 $^{\circ}C$ for 3.5 hours. The thermal oxidation layer is measured by the thin film measurement with a thickness of 740 $nm$ to provide enough electric insulation at high voltage. After that, the pillar pattern was lithographed and developed on to the wafer with photoresist (S1813, 1.26 $\mu m$). The Reactive Ion Etching (RIE) has been used to create hard mask for the Deep Reactive Ion Etching (DRIE) by etching the exposed oxidized layer from the previous lithograph process. Then the photoresist on the wafer was removed by the photoresist asher, and the wafer was etched by the DRIE to create pillar structures about 6 $\mu m$ high. To fabricate the bottom side of the patterned wafer, its pillar-side was protected by another plain wafer by bonding

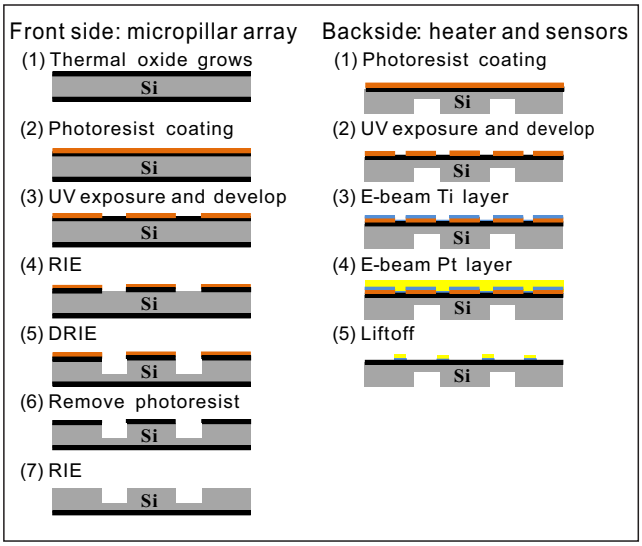


**FIGURE 3**. SUMMARY OF THE MICRO FABRICATION PROCESS OF THE FRONT AND BACK OF THE MICROPILLAR SAMPLES

them with Kapton tape at the edges. The patterns of the heater and resistance thermal detectors (RTDs) were lithographed with photoresist (S1813, 1.26 $\mu m$), and the wafer was deposited with 150 $nm$ of Ti and Pt by e-beam evaporation. Finally, the wafer was lifted off by using acetone to wash the excess photoresist away. The resistance of the heater and RTDs were designed to be around 200 Ω and around 700 Ω. The samples were diced to 1.7 mm by 2.0 mm with evaporation area of 1.0 $cm^2$ to leave some blank areas for mounting at two sides, as shown in the Fig. 4 (a). The heater and RTDs are shown in the Fig. 4 (b), and there are 10 contact pads for surface connections with pogo pins on the PCB. The Scanning electron micrographs (SEM) has been used to measure the actual diameter and height of the pillar, as shown in Fig. 4 (c) and (d). The parameters of the tested samples are shown in Table 1.

**TABLE 1**. PARAMETERS OF THE TEST SAMPLES

| | S1 | S2 | S3 |
|---|---|---|---|
| $d$ ($\mu m$) | 2.7 | 2.7 | 2.7 |
| $h$ ($\mu m$) | 6.4 | 6.4 | 6.4 |
| $l$ ($\mu m$) | 8 | 8 | 6 |
| $l_i$ ($mm$) | 0.625 | 0.5 | 0.5 |
| $w_i$ ($mm$) | 0.625 | 0.75 | 0.75 |

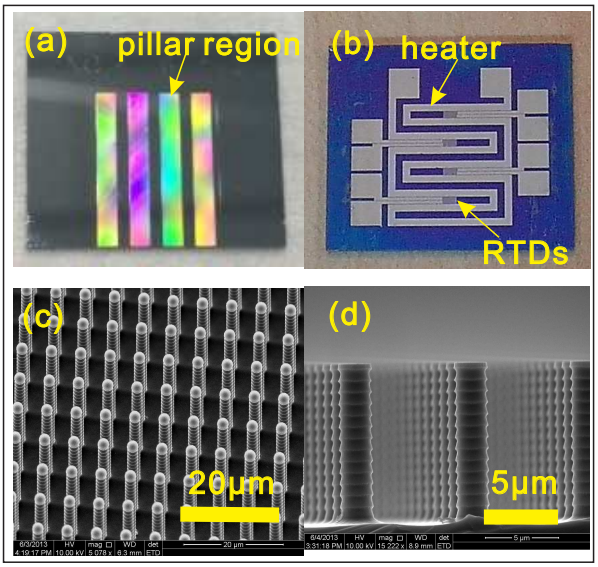


**FIGURE 4**. (A) MICROPILLAR ARRAY ON THE FRONT SIDE; (B) PLATINUM HEATER AND RTD ON THE BACK; (C) SEM IMAGES OF THE FABRICATED SAMPLE CAPTURED FROM 45 ° TILTED ANGLE; (D) SEM SIDE VIEWS.

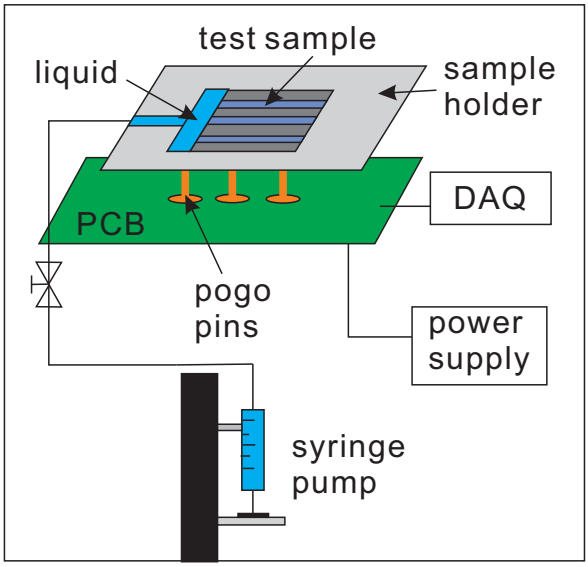


**FIGURE 5**. SUMMARY OF THE MICRO FABRICATION PROCESS OF THE FRONT AND BACK OF THE MICROPILLAR SAMPLES

## 2.2 Experimental setup

As shown in the Fig. 5, a 1D sample was mounted to the sample holder with two brackets at both sides to press down the sample to create a seal with the silicone gasket. The sample has been cleaned with acetone and isopropanol (IPA) and rinsed in the deionized (DI) water, and dried with $N_2$. After that, it was put into the plasma (Harrick Plasma PDC-002 ) for surface treatment in order to reduce its wetting contact angle to as low as 13°. The DI water pumped by the syringe pump (KDS Legato 110) flowed into the sample holder to form a liquid reservoir ($4 \times 3 \times 1$ $mm^3$) before reaching the sample to alleviate the flow variation caused by the syringe pump. The heater and RTDs were connected to the sample through 1.8 *mm* in-dia gold-plated pogo pin on the 1.6 *mm* thick PCB connection board. A DC power supply (GWInstek GPD-3303S) provided the heating power, and a data acquisition (DAQ) system (Keysight 34972A with 34902A board) were used to record the resistances of the RTD sensors. Before starting the experiments, the sample connected with DAQ have been put into a heating oven to calibrate the RTD sensors with a PT-100 thermometer (Omega), which has been calibrated with a Standard Platinum Resistance Thermometer (SPRT, Fluke) and a thermometer readout (Fluke 1560) with a uncertainty less than 0.1 $^\circ C$ by considering all the uncertain factors. After that, the mounted holder was placed on a weighting machine , and by controlling the pumping rate gently to form a thin film on the sample and monitoring the weight of the whole setup, if the weight of the whole setup has been stable within $\pm$ 20 *mg* for 1 minute, it is considering as a steady state. After data recording for 1 minute, the voltage would be increased 2.0 $V$ for another measurement. We noticed that when the DC voltage was higher than 25.0 $V$ during the experiments, there were some bubbles forming at the pillar area of the sample. Therefore the heating voltage was limited within 5.0 $V$ to 20.0 $V$ to ensure a steady evaporating condition, as the current model doesn't consider bubbles and boiling effects. The ambient condition is 27 $\pm$ 1 $^\circ C$ with a humidity of 80 $\pm$ 10 %. Three samples with the same number of channels have been tested in the current experiments, and the size of the evaporator of all the samples is 1 $cm^2$.

## 3 Results and discussions

The results of the experiments of the three sample are shown in the Fig. 6, which reflects the superheat changes with the supplied voltage. The superheat, $\Delta T$, is calculated from the temperature difference between the RTD sensors and the ambient. The general trend is the $\Delta T$ increases with the voltage.

The theoretical heat flux of the same three samples have been calculated from Eqn. (4). Since for each sample, the effective thermal conductivity, $k_{eff}$, can be calculated from $d, h, l$, which is a constant, and the details of the $k_{eff}$ has been modeled in [20]. By converting the voltage to the heating power on each sample, the relation between $\Delta T$ and heat flux, $q''$, is shown in the Fig. 7. With the same pillar island width, $l_i$, the sample with narrower pitch, $l$, which is shown as the triangle in the Fig. 7 has higher $q''$ at the same $\Delta T$ comparing with the line in circle. As

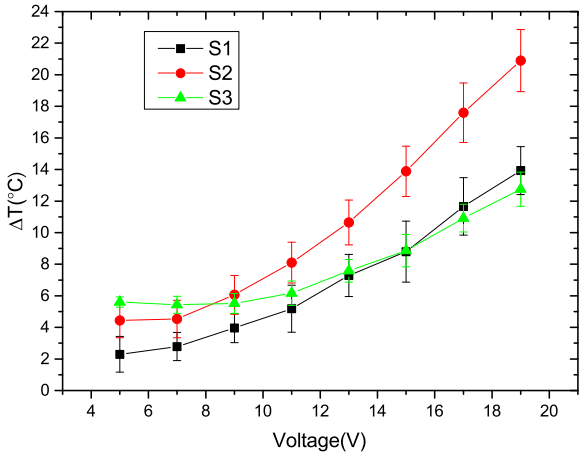


**FIGURE 6**. EXPERIMENTAL RESULTS OF SUPPERHEAT, $\Delta T$, WITH SUPPLIED VOLTAGE OF THE THREE TEST SAMPLES

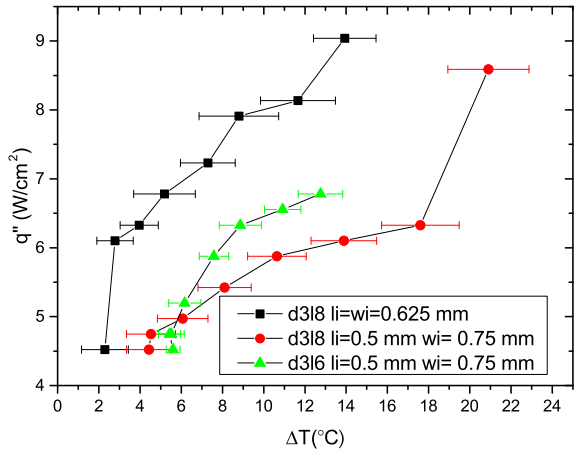


**FIGURE 7**. EXPERIMENTAL RESULTS OF HEAT FLUX, $q''$, WITH SUPPERHEAT, $\Delta T$, OF THE THREE TEST SAMPLES

a smaller pitch can provide more thin film area for evaporation which can promise a better performance. Additionally, the sample with larger $l_i$ on the sample has more effective evaporative pillar area since the evaporation inside the channel area is negligible, which demonstrates higher $q''$ at the same $\Delta T$ in the square symbol in the Fig. 7 than in circle symbol.

$$q'' = k_{eff} \frac{\Delta T}{h} \tag{4}$$

As shown in Fig. 8, the results show linear relationship between $\Delta T$ and heat flux, $q''$ according to the parameters of the three samples. Although the trend between Fig. 7 and Fig. 8 are generally the same, the experimental results have large performance gaps, which are $70 \sim 80$ %, to match the simulation results. The reasons may from the high humidity at the open experimental environment, and the inaccurate calculation of the $\Delta T$. The high humidity hinders the water from evaporation, which it is different from the modeled situation. The model suggests a vacuum condition inside a vapor chamber that can enhance the evaporation. Additionally, it is supposed to measure the temperature at the interface of the meniscus in order to calculate the temperature difference between the bottom RTDs to obtain the superheat. However, it is tricky to find and place a miniature temperature detector at this small region to acquire a reliable reading especially at high evaporation rate. Yet, such inaccuracy can be minimized if the experiments can be carried out at a vacuum chamber with good thermal insulation to control the system pressure and temperature for a steady reading. And in that case we

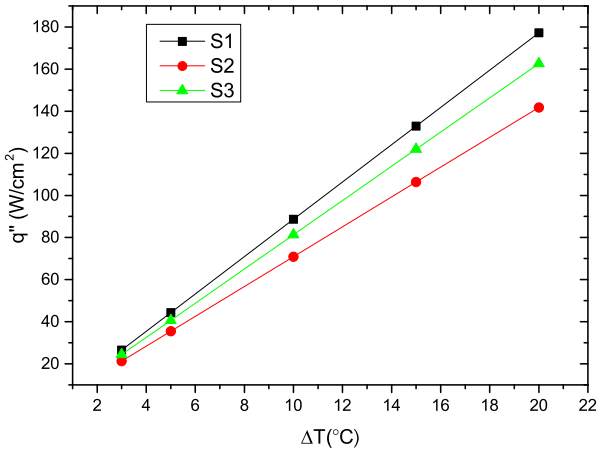


**FIGURE 8**. CALCULATION RESULTS OF HEAT FLUX, $q''$, WITH SUPPERHEAT, $\Delta T$, OF THE THREE SAMPLES

can assume the temperature reading of the vacuum chamber is about the same as that on the evaporation interface.

## 4 Conclusions

This paper presents the experimental investigations of the channeled sample to enhance the heat transfer performance of the pillared evaporator designed according to the analytical model. The experimental results show that the relationship between su-

perheat and heat flux in good trend with the modeled results. A smaller pitch can provide more thin film evaporation area and a wider evaporative pillar island can provide better heat transfer performance. The potential improvements of the experimental setup have been discussed as well.

## ACKNOWLEDGMENT

This research was supported by the National Research Foundaiton Singapore through Singapore MIT Alliance for Research and Technology's Low Energy Electronic Systems (LEES) IRG.

## REFERENCES

[1] Cai, Q., chung Chen, B., and Tsai, C., 2012. "Design, development and tests of high-performance silicon vapor chamber". *Journal of Micromechanics and Microengineering,* ***22***(3), p. 035009.

[2] Cai, Q., Bhunia, A., Tsai, C., Kendig, M. W., and DeNatale, J. F., 2013. "Studies of material and process compatibility in developing compact silicon vapor chambers". *Journal of Micromechanics and Microengineering,* ***23***(6), p. 065003.

[3] Cai, Q., Bhunia, A., Tsai, C., Kendig, M. W., and DeNatale, J. F., 2013. "Studies of material and process compatibility in developing compact silicon vapor chambers". *Journal of Micromechanics and Microengineering,* ***23***(6), p. 065003.

[4] Wang, H., Garimella, S. V., and Murthy, J. Y., 2007. "Characteristics of an evaporating thin film in a microchannel". *International Journal of Heat and Mass Transfer,* ***50***(1920), pp. 3933 – 3942.

[5] Wang, H., Garimella, S. V., and Murthy, J. Y., 2008. "An analytical solution for the total heat transfer in the thin-film region of an evaporating meniscus". *International Journal of Heat and Mass Transfer,* ***51***(2526), pp. 6317 – 6322.

[6] Ranjan, R., Murthy, J. Y., and Garimella, S. V., 2009. "Analysis of the wicking and thin-film evaporation characteristics of microstructures". *Journal of Heat Transfer,* ***131***(10), July, pp. 101001–101001.

[7] Ranjan, R., Patel, A., Garimella, S. V., and Murthy, J. Y., 2012. "Wicking and thermal characteristics of micropillared structures for use in passive heat spreaders". *International Journal of Heat and Mass Transfer,* ***55***(4), pp. 586 – 596.

[8] Li, H., Liu, Z., Chen, B., Liu, W., Li, C., and Yang, J., 2012. "Development of biporous wicks for flat-plate loop heat pipe". *Experimental Thermal and Fluid Science,* ***37***, pp. 91 – 97.

[9] Chen, B., Liu, W., Liu, Z., Li, H., and Yang, J., 2012. "Experimental investigation of loop heat pipe with flat evaporator using biporous wick". *Applied Thermal Engineering,* ***42***, pp. 34 – 40. Heat Powered Cycles Conference, 2009.

[10] Chen, B., Liu, Z., Liu, W., Yang, J., Li, H., and Wang, D., 2012. "Operational characteristics of two biporous wicks used in loop heat pipe with flat evaporator". *International Journal of Heat and Mass Transfer,* ***55***(78), pp. 2204 – 2207.

[11] Weibel, J. A., Garimella, S. V., and North, M. T., 2010. "Characterization of evaporation and boiling from sintered powder wicks fed by capillary action". *International Journal of Heat and Mass Transfer,* ***53***(1920), pp. 4204 – 4215.

[12] Byon, C., and Kim, S. J., 2012. "Capillary performance of bi-porous sintered metal wicks". *International Journal of Heat and Mass Transfer,* ***55***(1516), pp. 4096 – 4103.

[13] Cai, Q., and Chen, C.-L., 2010. "Design and test of carbon nanotube biwick structure for high-heat-flux phase change heat transfer". *Journal of Heat Transfer,* ***132***(5), Mar., pp. 052403–052403.

[14] Byon, C., and Kim, S. J., 2014. "Study on the capillary performance of micro-post wicks with non-homogeneous configurations". *International Journal of Heat and Mass Transfer,* ***68***, pp. 415 – 421.

[15] Wei, M., Somasundaram, S., He, B., Liang, Q., Tan, C. S., and Wang, E., 2014. "Experimental characterization of si micropillar based evaporator for advanced vapor chambers". In Electronics Packaging Technology Conference (EPTC), 2014 IEEE 16th, pp. 335–340.

[16] Wang, J., and Catton, I., 2001. "Evaporation heat transfer in thin biporous media". *Heat and Mass Transfer,* ***37***(2-3), pp. 275–281.

[17] Semenic, T., Lin, Y.-Y., and Catton, I., 2008. "Thermophysical properties of biporous heat pipe evaporators". *Journal of Heat Transfer,* ***130***(2), Feb., pp. 022602–022602.

[18] Semenic, T., Lin, Y. Y., Catton, I., and Sarraf, D. B., 2008. "Use of biporous wicks to remove high heat fluxes". *Applied Thermal Engineering,* ***28***(4), pp. 278 – 283. Heat Pipes, Heat Pumps and RefrigeratorsSelected Papers from the 6th Minsk International Seminar on Heat Pipes, Heat Pumps and Refrigerators.

[19] Semenic, T., and Catton, I., 2009. "Experimental study of biporous wicks for high heat flux applications". *International Journal of Heat and Mass Transfer,* ***52***(2122), pp. 5113 – 5121.

[20] Wei, M., Somasundaram, S., He, B., Liang, Q., Raj, R., Tan, C. S., and Wang, E., 2015. "Optimization of biporous micropillar array for enhanced heat transfer performance". In Proceedings of the ASME 2015 International Mechanical Engineering Congress & Exposition.

[21] Xiao, R., Enright, R., and Wang, E. N., 2010. "Prediction and optimization of liquid propagation in micropillar arrays". *Langmuir,* ***26***(19), pp. 15070–15075. PMID: 20806979.

[22] Brakke, K. A., 1992. "The surface evolver". *Experimental Mathematics,* ***1***(2), pp. 141–165.

[23] Liang, Q., Raj, R., Adera, S., Somasundaram, S., Tan, C. S., and Wang, E., 2013. "Experiment and modeling of microstructured capillary wicks for thermal management of electronics". In Electronics Packaging Technology Conference (EPTC 2013), 2013 IEEE 15th, pp. 592–597.